Geochemistry, Geophysics, Geosystems

RESEARCH ARTICLE
10.1029/2019GC008364

Interpretation of Late-Pleistocene/Holocene Transition in the Sea of Marmara From Geochemistry of Bulk Carbonates

Yujia Liu[1], Hailong Lu[1], Xijie Yin[2], Livio Ruffine[3], M. Namik Çağatay[4], Hailin Yang[1], Chunqing Chen[2], Dong He[5], Zhenli Zhu[5], and Burak Yalamaz[4]

[1]Beijing International Center for Gas Hydrate, and College of Engineering, Peking University, Beijing, China, [2]The 3rd institute of Oceanography, State Oceanic Administration, Xiamen, China, [3]Ifremer, Département Ressources physiques et Ecosystèmes de fond de Mer (REM), Unité des Géosciences Marines, Laboratoire des Cycles Géochimiques et ressources (LCG), Plouzané, France, [4]EMCOL Research Centre, Istanbul Technical University, Istanbul, Turkey, [5]State Key Laboratory for Biogeology and Environmental Geology, China University of Geosciences, Wuhan, China

Key Points:
- The geochemical characteristics of bulk carbonates imply the lacustrine/marine transition across the Late Pleistocene/Holocene
- Subsurface biodegradation of petroleum was evidenced by the geochemical characteristics of bulk carbonates
- Primary carbonates were dissolved in the acidic environment and authigenic carbonates precipitated

Supporting Information:
- Supporting Information S1

Correspondence to:
H. Lu,
hlu@pku.edu.cn

Citation:
Liu, Y., Lu, H., Yin, X., Ruffine, L., Çağatay, M. N., Yang, H., et al. (2019). Interpretation of Late-Pleistocene/Holocene transition in the Sea of Marmara from geochemistry of bulk carbonates. *Geochemistry, Geophysics, Geosystems*, *20*, 4487–4504. https://doi.org/10.1029/2019GC008364

Received 8 APR 2019
Accepted 28 AUG 2019
Accepted article online 11 SEP 2019
Published online 16 OCT 2019

Abstract Isotopic, mineralogical, and elemental analyses have been conducted for the geochemical characteristics of the bulk carbonates in the sediment cores from the Western High and Çınarcık Basin in the Sea of Marmara to investigate the authigenic, biogenic, and detrital components and their possible use in paleoceanographic studies. The Western High is a relatively shallow (−500 to −800 m) compressional area characterized by relatively low sedimentation rates (30–40 cm/Kyr), whereas the Çnarcık Basin is a deep (~1,250 m) transtentional area represented by high sedimentation rates (>1 m/Kyr). Both $^{87}Sr/^{86}Sr$ and $\delta^{18}O$ of bulk carbonates from the Western High exhibit significant variations, increasing steeply from $^{87}Sr/^{86}Sr$ of 0.708437 to 0.708916 and $\delta^{18}O$ of −3.2‰ Vienna Pee Dee Belemnite (VPDB) to 0.1‰ VPDB, indicating the incursion of the Mediterranean seawater after the last glacial and reflected in the change from lacustrine to marine environment. However, bulk carbonates in the core from the Çınarcık Basin have comparatively uniform values of $^{87}Sr/^{86}Sr$ (~0.708845) and $\delta^{18}O$ (~0.0‰ VPDB), implying that this core did not experience the lacustrine/marine transition. In the Western High, $\delta^{13}C$ values up to +24.3‰ VPDB at 400 cm below seafloor reveal the mineralization of heavy CO_2, providing independent evidence for the subsurface biodegradation of petroleum. While in the Çınarcık Basin, $\delta^{13}C$ values of bulk carbonates were relatively constant (approximately −2.94‰ VPDB). The high $\delta^{13}C$ values of bulk carbonates from the Western High reflect the dissolution of primary carbonates as a result of the local acidic environment and precipitation of authigenic carbonates later, supported by mineralogical and elemental results.

Plain Language Summary Bulk carbonates in two sediment cores from the Western High and the Çınarcık Basin in the Sea of Marmara are investigated to determine their origin and their paleoceanographic significance. The $^{87}Sr/^{86}Sr$ and $\delta^{18}O$ results of the bulk carbonates from the Western High reveal an incursion of the Mediterranean seawater after the Last Glacial Maximum, while the comparatively uniform geochemical values of the bulk carbonates in the core from the Çınarcık Basin imply that this core did not experience the lacustrine/marine transition. In the Western High, the acidic environment in the sediments was likely caused by migration of petroleum that biodegraded anaerobically close to its migration depth. The acidic environment first led to the dissolution of primary carbonates, after which authigenic carbonates precipitated. The mixing model based on element ratios of Sr/Ca and Mg/Ca suggests that the major components of bulk carbonates are authigenic aragonite and high Mg-calcite in the Western High, while the major components of bulk carbonates are biogenic and detrital calcite in the Çınarcık Basin.

1. Introduction

The carbonates in marine sediments commonly consist of mixed sources with authigenic, biogenic, and detrital origins. Authigenic carbonates associated with cold seeps are found in various marine settings, including active and passive margins, and silled marine basins (Birgel et al., 2011; Çağatay et al., 2017; Chevalier et al., 2011; Crémière, Pierre, et al., 2012; Crémière et al., 2013; Pierre et al., 2016). The cold seep authigenic carbonates are produced from anaerobic oxidation of methane (AOM), which is operated by anaerobic methane-oxidizing archaea and sulfate-reducing bacteria (Boetius et al., 2000; Hinrichs et al., 1999; Orphan et al., 2001). Microbial degradation of organic matter and thermogenic processes produce fluids

enriched in methane and other hydrocarbons (Whiticar, 1999). The methane-rich fluids migrate upward and react with the sulfate-rich interstitial seawater at the sulfate-methane transition zone (Borowski et al., 1996). The bicarbonate generated by AOM increases the alkalinity of pore water and favors the precipitation of authigenic carbonates according to the following reactions (Aloisi et al., 2000; Çağatay et al., 2017; Crémière et al., 2013).

$$CH_4 + SO_4^{2-} \rightarrow HCO_3^- + HS^- + H_2O$$
$$2HCO_3^- + Ca^{2+} \rightarrow CaCO_3 + CO_2 + H_2O.$$

Thermogenic gases are relatively enriched in C_2 compared to biogenic gases, with $C_1/C_2 + C_3$ ratios below 1,000, and biogenic gases have increased $C_1/C_2 + C_3$ ratios (>10,000). As for $\delta^{13}C$, thermogenic gases are composed mainly of isotopically heavier methane ($\delta^{13}C_{CH4} > -57‰$), while biogenic methane is depleted in ^{13}C ($\delta^{13}C_{CH4} < -57‰$; Claypool & Kvenvolden, 1983). On the Western High, the methane contained in free gas and gas hydrate is primarily thermogenic, as recognized from $\delta^{13}C_{CH4}$ of −46.35‰ Vienna Pee Dee Belemnite (VPDB) and $C_1/C_2 + C_3$ ratio of 24.4–3.3 (Bourry et al., 2009; Ruffine et al., 2018). Heavy gases from C_2 to C_5 with $\delta^{13}C$ of −29.95‰ to −20.85‰ VPDB and CO_2 with $\delta^{13}C$ of 28.4‰ to 29.1‰ VPDB are also present in relatively high content (Ruffine, Donval, et al., 2018). Gases collected from the Western High contain 90.90% CH_4, 1.23% C_2, 2.50% C_3, 0.93% i-C_4, 0.15% n-C_4, 0.31% i-C_5, and 3.90% CO_2 (Bourry et al., 2009). The composition of gas from the Western High has high similarity with that from the *K.Marmara-af* gas field, suggesting part of the fluids expelled on the Western High originates from the hydrocarbon source rocks of Thrace Basin (Bourry et al., 2009; Gürgey et al., 2005). Unlike CO_2 in the *K.Marmara-af* gas field with a low $\delta^{13}C$ value of −5.71‰ VPDB, CO_2 found in the Western High evidence subsurface biodegradation of petroleum with high $\delta^{13}C$. Besides, the petroleum from the Thrace Basin hydrocarbon source rocks also migrates along the active faults (Bourry et al., 2009; Dupré et al., 2015; Gürgey et al., 2005). On the other hand, methane in the Çınarcık Basin, with a $\delta^{13}C_{CH4}$ of −66.05‰ VPDB and a $C_1/(C_2 + C_3)$ ratio of 16,600, is primarily of microbial origin (Bourry et al., 2009; Ruffine, Donval, et al., 2018; Zitter et al., 2008).

The carbon isotopic composition of carbonates can provide useful information on their carbon sources. Dissolved inorganic carbon (DIC), from which carbonates precipitated, could originate from either AOM or biodegradation of crude oil (petroleum) in subsurface petroleum reservoirs (Jones et al., 2008). The oxygen isotopic composition of carbonate is influenced by both the temperature and the water $\delta^{18}O$ of aqueous solutions from which the carbonates precipitate (Crémière, Pierre, et al., 2012; Deuser, 1972; Friedman and O'Neil, 1977; Pierre et al., 2016; Vidal et al., 2010).

Seafloor authigenic carbonate crusts have been studied in detail in the Sea of Marmara (SoM; Çağatay et al., 2017; Chevalier et al., 2011; Crémière et al., 2012; Crémière et al., 2013; Crémière, Pierre, et al., 2012). Since cold seeps characterized by methane-rich gas venting are widespread all along the North Anatolian Fault System (Armijo et al., 2005; Chevalier et al., 2011; Crémière et al., 2013; Crémière, Pierre, et al., 2012; Ruffine et al., 2015), the geochemical data of seafloor authigenic carbonates can provide information about various processes including seismo-tectonic activity, gas hydrates destabilization (Çağatay et al., 2017; Teichert et al., 2018), and changes in fluid source and DICs (Chevalier et al., 2011). Authigenic carbonates in the deep basins have lighter $\delta^{18}O$ values (0.5‰ to 3.8‰ VPDB) because of the emissions of brackish "Lake" water and lower $\delta^{13}C$ values (−47.6‰ to −13.7‰ VPDB) resulting from the anaerobic oxidation of both microbial and thermogenic methane. On the other hand, the seafloor carbonates from the compressional highs are characterized by relatively high $\delta^{18}O$ (2.6‰ to 3.4‰ VPDB) and $\delta^{13}C$ (−13.7‰ to 24.9‰ VPDB) values, due to various processes and sources of fluids, including emission of deep saline formation water from the Thrace Basin, gas hydrate dissociation, thermogenic methane, and biodegradation of heavy hydrocarbons (Bourry et al., 2009; Çağatay et al., 2017; Crémière, Pierre, et al., 2012; Tryon et al., 2010).

Temporal changes in the oxygen and strontium isotopic compositions of biogenic carbonates have been used for numerous paleoceanographic reconstructions (Aksu et al., 2002; Bahr et al., 2006; Çağatay et al., 2006; Israelson & Buchardt, 1999; Major et al., 2006; Vidal et al., 2010). This is especially relevant for the SoM, where the oxygen and strontium isotopic compositions of biogenic carbonates can be applied to the investigation of the hydrologic evolution in relation to the connection with the Mediterranean and the Black Sea. The SoM was under lacustrine conditions until the establishment of the latest marine conditions at 12.55

± 0.35 cal ka BP (Çağatay et al., 2015), with the initial marine incursion occurring somewhat earlier, at ~14.7 cal ka BP (Vidal et al., 2010). Because of the change from lacustrine to marine conditions, the Late Glacial to Holocene sedimentary succession in the SoM can be subdivided into an upper marine and a lower lacustrine units (Çağatay et al., 2000; Eriş et al., 2012; Vidal et al., 2010). This transition is clearly indicated by the change in the Sr isotopic ratios of mollusk shells in Core MD01-2430 on the Western High in the SoM, which range from 0.70898 for the lacustrine species to 0.70916 for the marine species (Vidal et al., 2010). In parallel with this, the $\delta^{18}O$ record of benthic ostracods also shows an increase of approximately 3‰ across the lacustrine/marine transition (Vidal et al., 2010). Such geochemical records in unconsolidated sediments were typically generated through measurements on biogenic carbonates such as foraminifera, bivalves, and mollusk shells.

Up to now, only a few studies have been carried out on the bulk carbonates of unconsolidated sediments in the SoM and the adjacent Black Sea (Cox & Faure, 1974; Deuser, 1972; Major et al., 2002). This is because the bulk carbonate fractions could include primary biogenic carbonates reflecting the paleoenvironment, detrital (reworked) carbonates transported from the catchment, and authigenic carbonates formed during or after the sedimentation, thus complicating the interpretations. For example, stable oxygen and carbon isotopic ratio changes of reworked to endogenic carbonate fractions in bulk carbonates of the Core 1474K in the Black Sea lead to multiple possibilities in interpreting the results for environmental reconstructions (Deuser, 1972). The incursion of high-salinity Mediterranean water into the Black Sea through the SoM caused an increase in $\delta^{18}O$ of mollusk shells in Core BLKS9810, while the stratification in the water column, brought about by the incursion of denser water, also resulted in a decrease in $\delta^{18}O$ of the bulk carbonate of the sediment (Major et al., 2002). As for strontium isotopes, $^{87}Sr/^{86}Sr$ of bulk carbonate in the lower part of Core 1447P displays low values caused by the inclusion of the reworked Late Cretaceous-Neogene coccoliths (Cox & Faure, 1974).

In this paper, we report the analytical results of bulk carbonates in two sediment cores collected from two important morphotectonic provinces in the SoM: the Western High and the Çınarcık Basin. The Western High is a compressional area characterized by seepage of thermogenic methane and heavy hydrocarbons, presence of gas hydrate, and relatively low sedimentation rates (30–40 cm/Kyr), whereas the Çınarcık Basin is one of the three deep (~1,250 m) transtentional subbasins, represented by emission of mainly biogenic methane and high (>1 m/Kyr) sedimentation rates (e.g., Armijo et al., 2002; Çağatay & Ucarkus, 2018; Ruffine et al., 2018; Zitter et al., 2008). To investigate the origin of the bulk carbonates in the two sediment cores from the Western High and the Çınarcık Basin, we analyzed the bulk carbonates for their stable carbon and oxygen isotopic and mineral compositions, together with the elemental concentrations and strontium isotopes in the selectively dissolved solutions of carbonates in chosen sediment samples. The results obtained are used to investigate past water exchanges between the two neighboring seas, the Black Sea and the Mediterranean Sea, and to provide information about the anaerobic biodegradation of petroleum in subsurface sediments. Processes related to the dissolution of primary carbonates and the precipitation of authigenic carbonate minerals are also discussed.

2. Geological Setting

The SoM is a 210-km-long and 75-km-wide intracontinental sea located in the Turkish territory and crossed from east to west by the North Anatolian Fault (Figure 1). It includes three ~1,250-m-deep basins, which from west to east are called the Tekirdağ Basin, Central Basin, and Çınarcık Basin. These basins are separated by the Western and the Central highs (Rangin et al., 2001; Figure 1). The Çınarcık Basin is the largest and deepest basin (1,265 m deep) and appears as an active pull-apart basin formed across a large releasing bend/step over between the main strike-slip faults of the North Anatolian Fault (Armijo et al., 2002). The Western High consists of more than 6-km-thick sedimentary sequence (Bayrakci et al., 2013), which comprises Eocene-Miocene sedimentary rocks of the Thrace Basin in the lower portion (Görür & Elbek, 2013). The Holocene sedimentation rate in the deep basins such as the Çınarcık Basin is higher (1–2 m/Kyr) compared to that on the compressional highs (~0.2–0.5 m/ka; Çağatay et al., 2009; Çağatay et al., 2000).

The SoM constitutes a gateway connecting the brackish Black Sea (18–22 psu) and the saline Aegean Sea (37.5–38.5 psu), through the straits of Bosphorus (~35 m deep) and Dardanelles (~65 m deep), respectively (Çağatay et al., 2000; Çağatay et al., 2009; Kirci-Elmas et al., 2008). The topographical restrictions (sill

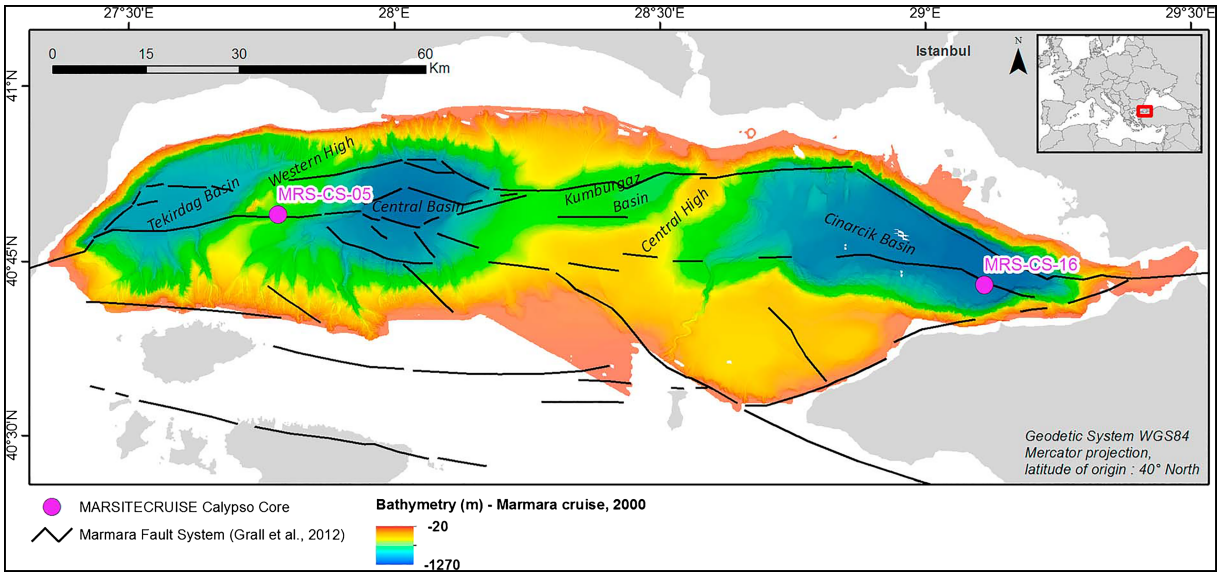

Figure 1. Bathymetric map of the Sea of Marmara with the positions of the cores discussed in the text.

depth) of both straits control the water exchanges between the Black Sea and the Aegean Sea, causing disconnections during glacial lowstands and connections during the interglacial periods. Major rivers including Biga, Gönen, and Kocasu flow into the SoM from the south with a sediment discharge of 2.2 × 10^6 t/year and a freshwater discharge of 5.8 km^3/year (Çağatay et al., 2000; EIE., 1993). This riverine freshwater discharge is much less than the brackish water influx of 605 km^3/year from the Black Sea (Hiscott & Aksu, 2002; Hiscott et al., 2002) and the saline water influx of 376 km^3/year from the Aegean Sea (Özsoy & Ünlüata, 1997; Ünlülata et al., 1990).

3. Materials and Methods

3.1. Sampling Sites

Two gravity cores were collected during the MARSITE cruise expedition onboard the R/V *Pourquoi pas?* in November 2014 (Table 1 and Figure 1). The Cores MRS-CS-05 and MRS-CS-16 were collected from the Western High and Çınarcık Basin at water depths of 657 and 1,237 m, respectively (Table 1). Each of the two cores was cut into 1-m-long sections, split in two halves, and systematically subsampled at 100-cm intervals.

3.2. Lithology

3.2.1. Lithology of Core MRS-CS-05 (Western High)

The 867-cm-long sedimentary sequence MRS-CS-05 from the Western High consists of two units: a 316-cm-thick upper marine unit and an underlying lacustrine unit (Figure 2a). The upper 0–79 cm below seafloor (cmbsf) part of the marine unit is dark green gray silty clay. This portion has a porous, brecciated structure resulting from gas hydrate dissociation and a strong smell of H_2S. The lower part of the unit between 79 and 305 cmbsf is a sapropel containing up to 1.8 wt.% total organic carbon (TOC), which is clearly higher than that of 1.2 wt.% for the lacustrine unit below (Yang et al., 2018; Figure 2a). This sapropel layer (305–316 cmbsf) corresponds to the Holocene sapropel layer previously described in the SoM (Çağatay et al., 2000; Çağatay et al., 2015). The transition to the lacustrine unit below is characterized by the reddish brown mud from 316 to 350 cmbsf, with some carbonate patches (Figure 2a). The reddish-brown color is attributed to the oxidation of Fe-sulfide, after the core was exposed to the atmosphere. The carbonate-rich transition layer indicates the precipitation of carbonates by mixing of anoxic deep lacustrine water with oxic Mediterranean water (Reichel & Halbach, 2007). The lacustrine unit from 350 to 867 cmbsf contains gray to dark gray silty clay, with carbonate-rich bands. In most part, the lacustrine unit is strongly disturbed with brecciated and soupy structures, which can be attributed to gas hydrate dissociation and the release of the

Table 1
Location and Length of Studied Cores

Core	Location	Latitude	Longitude	Length (cm)	Water depth (m)
MRS-CS-05	Western High	N40°49.03′	E27°46.85′	867	657
MRS-CS-16	Çınarcık Basin	N40°49.98′	E29°6.70′	1,012	1,237

enclathrated gases. It is also commonly impregnated by petroleum and contains patches of centimeter-size authigenic carbonates (Figure 2a).

3.2.2. Lithology of Core MRS-CS-16 (Çınarcık Basin)

The sedimentary sequence in Core MRS-CS-16 from the Çınarcık Basin comprises only the upper marine unit (Figure 2b). The unit consists of a hemipelagic greenish gray mud sequence that is interrupted by numerous 1- to 12-cm-thick sandy turbidites and up to 13-cm-wide gas expansion voids. The marine unit includes a sapropel starting from ~100 cmbsf extending all the way to the core bottom. The sapropel is composed of dark olive green to greenish gray, laminated clay to silty clay. The TOC contents of the entire core, including the sapropel, is uniformly low with an average value of 1.2 wt.% (Yang et al., 2018). The low TOC values result from dilution of the organic carbon by a high detrital influx into the deep basin. The intercalated turbidite sand layers commonly have an erosional base and gradational to sharp upper contacts. The sands are usually enriched in white shell fragments. The gas voids in the lower part of the core are located in the porous turbidite sand beds.

3.3. PXRD Mineralogical

Sediment was analyzed for mineral identification by powder X-ray diffraction (PXRD) at Peking University. The samples were first dried and then powdered to less than 10 μm in an agate mortar. The prepared sediment powders were analyzed by a powder X-Ray diffraction (PANalytical Empyrean) with PIXcel1D-Medipix3 detector using Cu Kα radiation with the generator operated at 40 mA and 40 kV. Scans were collected over the 2θ range of 5–80°using a step size of 0.01°and a count time of 5 s per step.

3.4. Stable Oxygen and Carbon Isotope Analyses

The $\delta^{13}C$ and $\delta^{18}O$ were measured for bulk carbonate fraction of sediments using an automated carbonate-preparation device (GasBenchII) coupled with a stable isotope ratio mass spectrometer (Thermo Delta V Advantages) at the Laboratory of Ocean and Coast Geology, Third Institute of Oceanography State Oceanic Administration (Xiamen, China). Powdered samples (0.1 g) were reacted with dehydrated phosphoric acid under vacuum at 70 °C for 60 min to extract the carbonate fractions. Isotopic ratios are expressed in δ-

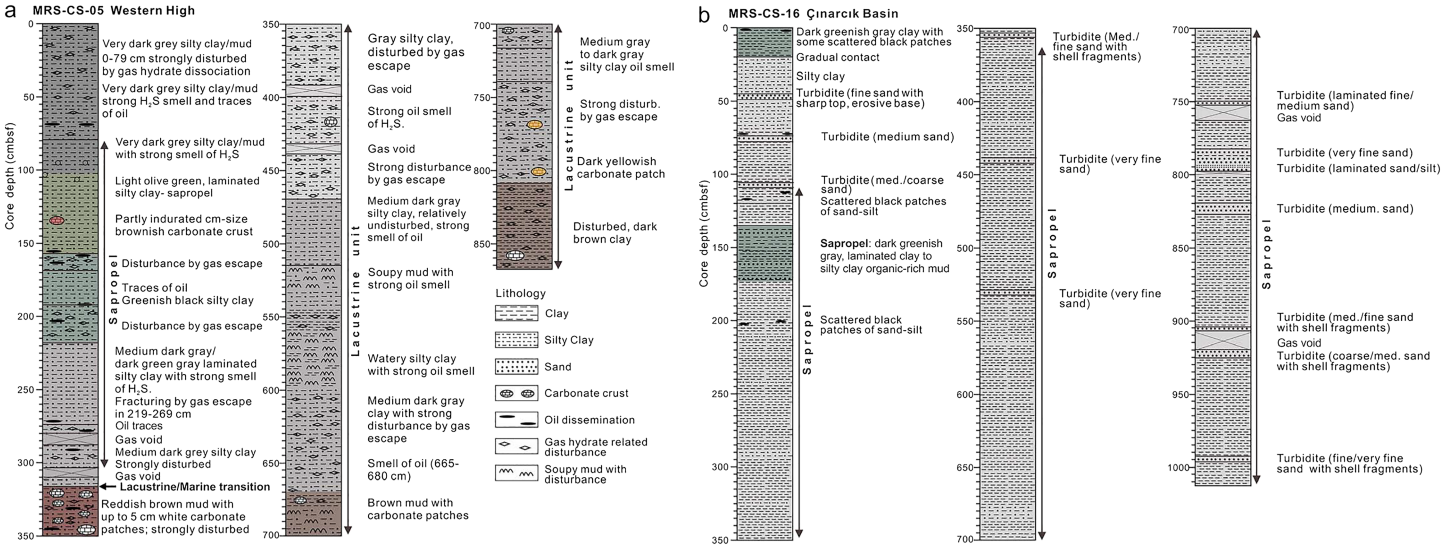

Figure 2. Lithological descriptions of (a) Core MRS-CS-05 from the Western High and (b) Core MRS-CS-16 from the Çınarcık Basin of the Sea of Marmara.

notation as per mil (‰) deviation relative to VPDB standard. The analytical precision of both $\delta^{13}C$ and $\delta^{18}O$ were smaller than 0.2‰.

3.5. Extraction of Carbonate Phase

A sequential selective extraction method modified from the procedure of Tessier et al. (1979) was applied for carbonate extraction (Table 2). The samples were first washed with deionized water to remove the sea salts, followed by a 1M NaAc reagent (pH 7.9) treatment for the extraction of exchangeable elements. Finally, the sediment samples after the first two steps were treated with 1M HAc reagent (pH 2.3) for the extraction of carbonate phases. Elemental concentrations and $^{87}Sr/^{86}Sr$ were measured only in the 1M HAc-extractable dissolved carbonates, and the supernatants from the first two extractions were discarded.

3.6. Inductively Coupled Plasma Optical Emission Spectrometer Analysis

Ca, Mg, Fe, Mn, and Sr concentrations were measured with a Spectro Blue Sop Inductively Coupled Plasma Optical Emission Spectrometer at Peking University. The extracted supernatant was diluted 50 times to around the concentration range of the standard solutions. The calibration curves were constructed by a series of gravimetric standard solutions with a concentration range of 0.1–10 ppm. Elemental concentrations were calculated on the basis of the original mass, with a precision better than 5%.

3.7. Multicollector Inductively Coupled Plasma Mass Spectrometer Analysis

Sr was extracted by on-column chromatography using Sr-spec resin (SR-B25-S resin, 50–100 μm; Wall et al., 2013). $^{87}Sr/^{86}Sr$ ratios were measured on Nu plasma Multicollector Inductively Coupled Plasma Mass Spectrometer at State Key Laboratory of Biogeology and Environmental Geology, China University of Geosciences (Wuhan). The supernatants extracted from the sequential extractions of carbonate-bound elements were dried, then digested with concentrated HNO_3, and finally dissolved in 3.5 M nitric acid. Two standards (U.S. Geological Survey basalt standard BHVO-2 and Strontium Carbonate Isotopic Standard SRM987) were processed together with the samples for the validation of the chemical extraction and the isotopic measurement. To ensure the analytical precision, the standards were run once every three samples. The external reproducibility (2σ) of $^{87}Sr/^{86}Sr$ measurements was below ± 0.00003, as assessed by repeated measurements of the above standards to match sample concentration. The $^{87}Sr/^{86}Sr$ ratio was normalized using $^{86}Sr/^{88}Sr$ of 0.1194 (Neymark et al., 2014).

3.8. SEM

Samples were mounted on stubs with the conductive silver adhesive and coated with chromium. Scanning electron microscope (SEM) imaging and energy diffraction spectrum of selected areas were carried out using an FEI Quanta 650 FEG SEM with the best resolution of 2.5 nm at the Key Laboratory of Orogenic Belts and Crustal Evolution, Peking University. The observation was operated at 10 kV, beam spot diameter 5.0 μm, and an SEM image of a certain range was taken in 10–20 μs for this research.

3.9. Mixing Model Based on Sr/Ca and Mg/Ca

The mixing model between four end-members (aragonite, high-Mg calcite, biogenic calcite, and detrital) was modified from the procedure of Bayon et al. (2007). The X and Y ordinates are Mg/Ca (mol/mol) and $Sr/Ca \times 10^3$ (mol/mol), respectively. The values of aragonite and Mg-calcite are cited from seafloor carbonates in the SoM (Çağatay et al., 2017), and the values for biogenic calcites are cited from foraminifera in the SoM (Fontanier et al., 2018). Each member is connected under exponential coordinates. Samples with different origin would fall into different regions between these lines.

4. Results

4.1. Mineralogical Composition From XRD Measurements and SEM Observations

The main mineral phases of the two sediment cores are clay minerals (smectite, illite, kaolinite, and chlorite), quartz, plagioclase, and carbonate minerals (Figure 3), as reported also by the previous mineralogical studies in the same area (Reichel & Halbach, 2007). The most frequent and PXRD-detectable carbonate mineral is calcite (2-Theta: 29.404, rruff.info/R040070) followed by siderite (2-Theta: 52.93, rruff.info/R050349). High-Mg calcite and aragonite are below the detection limit of the PXRD method (Figure 3) but identified in the SEM observations (Figure 4). Aragonite occurs as acicular crystals (Figures 4a and S1 in the

Table 2
The Sequential Extraction Procedure

Step	Fraction	Reagents	Solid/solution (volume)	pH	Reaction time (hr)	Temperature (°C)
1	Soluble	Deionized water	1:100	7	2	25
2	Exchangeable	1M NaAc	1:100	7.9	1	25
3	Carbonate minerals	1M HAc	1:100	2.3	16	25

supporting information), siderite as blade-like crystals (Figures 4b and 4c), and high-Mg calcite as platy crystals (Figure S2).

The calcite content varies significantly from one horizon to another in Core MRS-CS-05 (Figure 3a), while it is with few changes in Core MRS-CS-16 (Figure 3b). The peaks of calcite almost disappear at 100, 200, and 400 cmbsf in Core MRS-CS-05 but become stronger in other intervals (Figure 3a).

4.2. Oxygen and Carbon and Isotopic Composition

The stable carbon and oxygen isotopic composition of the bulk carbonate fraction ($\delta^{13}C_{bulk\ carbonate}$ and $\delta^{18}O_{bulk\ carbonate}$) in the studied cores are presented in Figures 5. The $\delta^{13}C_{bulk\ carbonate}$ values measured in

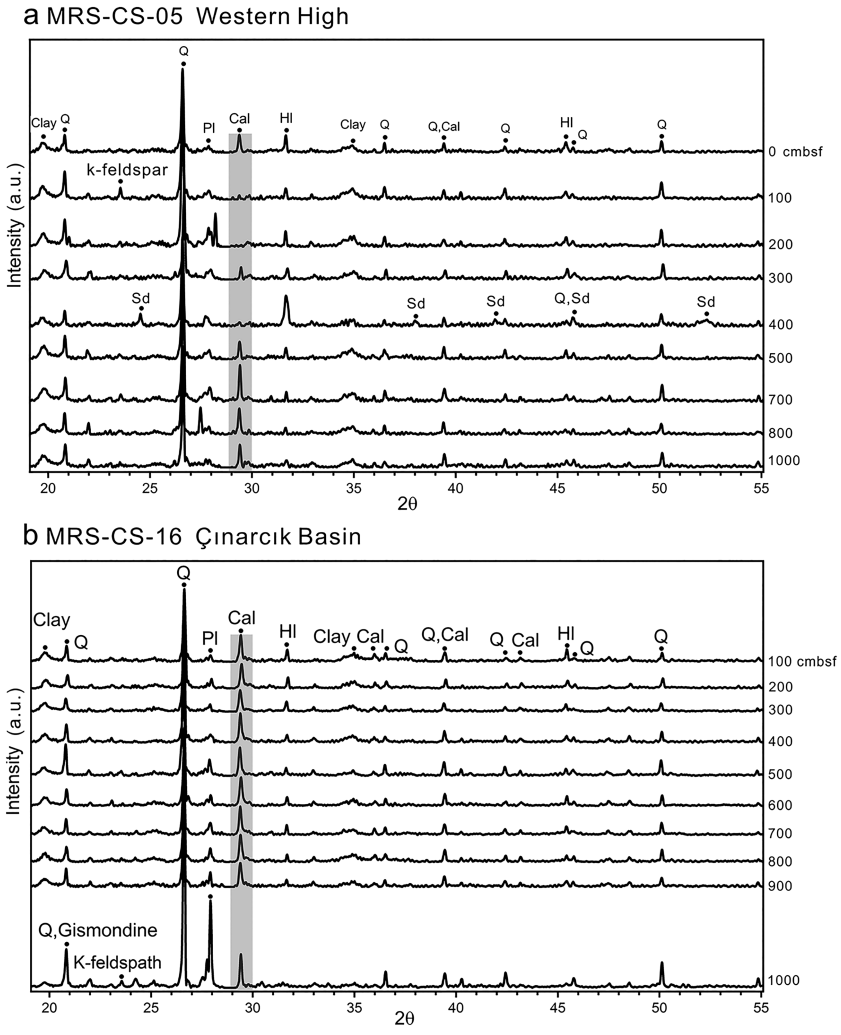

Figure 3. Powder X-ray diffractograms of sediments from (a) Core MRS-CS-05 and (b) Core MRS-CS-16 from the Sea of Marmara. Q = quartz; Pl = plagioclase; Hl = Halite; Cal = calcite; Sd = siderite.

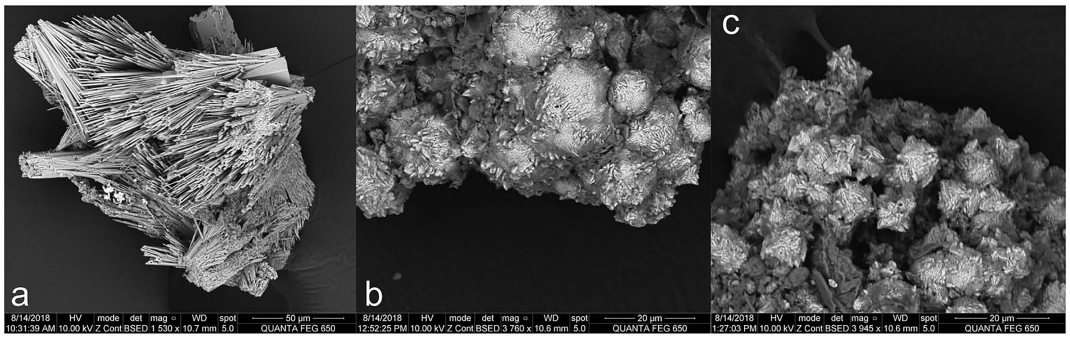

Figure 4. Scanning electron microscope microphotograph of authigenic carbonates in sediments from the Western High of the Marmara. (a) Acicular aragonite and (b,c) siderite formed on the surface of oxidized Fe sulfide.

Core MRS-CS-05 increase steadily from −0.92‰ at 1,000 cmbsf to 3.20‰ at 500 cmbsf and then shift abruptly to a notable enrichment of 24.30‰ at 400 cmbsf. After a minor depletion to −1.65‰ at 300 cmbsf, the $\delta^{13}C_{bulk\ carbonate}$ values vary slightly around −3.24‰ throughout the upper portion of the core. However, the $\delta^{13}C_{bulk\ carbonate}$ display relatively constant light values across Core MRS-CS-16, ranging from −3.86‰ to −1.53‰.

$\delta^{18}O_{bulk\ carbonate}$ values measured in Core MRS-CS-05 exhibit the heaviest value of 0.91‰ at 1,000 cmbsf and then show a transition by a small step-like depletion to the lightest value of −4.33‰ at 500 cmbsf. Above 500 cmbsf, the $\delta^{18}O_{bulk\ carbonate}$ values display a progressive enrichment up to 0.12‰ at 300 cmbsf. In the upper portion of the core from 200 cmbsf to the seafloor, the $\delta^{18}O_{bulk\ carbonate}$ values show negative excursions again to about −2.78‰. The upward variation of $\delta^{18}O_{bulk\ carbonate}$ in Core MRS-CS-16 displays a relatively uniform trend, starting with the minimum value of −1.28‰ at the bottom and then increasing progressively to the maximum value of 0.87‰ at 200 cmbsf in the upper portion.

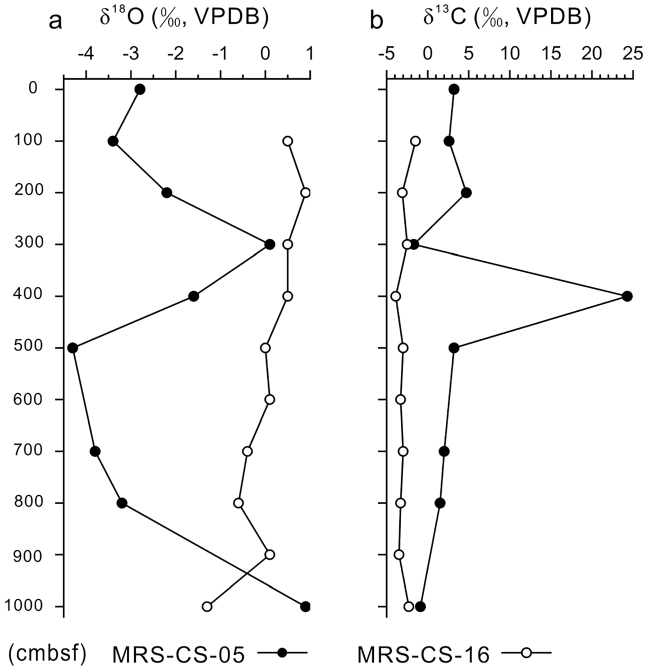

Figure 5. Oxygen and carbon isotopic compositions from Cores MRS-CS-05 and MRS-CS-16 from the Sea of Marmara. Filled and open circles represent the two cores, respectively. cmbsf = centimeters below seafloor; VPDB = Vienna Pee Dee Belemnite.

4.3. Carbonate-Bound Elements

Ca, Mg, Fe, and Mn concentrations and Ca/Mg of the bulk carbonate are plotted in Figure 6. For Core MRS-CS-05, Ca concentration exhibits a notable enrichment of 60.86 mg/g at 1,000 cmbsf and then decreases dramatically to 26.85 mg/g at 800 cmbsf. Above 800 cmbsf, Ca concentration drops continuously to 7.93 mg/g at 400 cmbsf. The most noteworthy features in the upper portion are the two extremely low values of 2.09 and 5.26 mg/g at depths of 200 and 100 cmbsf, respectively. Contrarily, Ca concentration displays a relatively steady trend in Core MRS-CS-16. It fluctuates around a mean value of 42.33 mg/g from the bottom to 600 cmbsf and then decreases to the minimum value of 31.87 mg/g at 500 cmbsf. Above 300 cmbsf, it fluctuates evenly about a value of 38.86 mg/g to the seafloor.

Parallel to the profile of Ca, Mg profile also displays significant variations in Core MRS-CS-05. It starts with a peak of 3.58 mg/g at the bottom of the core and then decreases sharply to 1.58 mg/g at 800 cmbsf. From 800 cmbsf to the seafloor, the Mg concentration varies slightly around 1.65 mg/g, except for two obvious negative excursions to 1.13 and 1.25 mg/g at 200 and 100 cmbsf. For Core MRS-CS-16, Mg concentration increases steeply from 2.09 mg/g at 1,000 cmbsf to 3.39 mg/g at 900 cmbsf. They increase further progressively to a significantly high value of 4.05 mg/g at 600 cmbsf, followed by a decrease to 3.22 mg/g at 500 cmbsf and an increase gradually to 3.94 mg/g at 100 cmbsf. It is worth noting that both Ca and Mg concentrations are higher in Core MRS-CS-16 than Core MRS-CS-05.

Fe and Mn concentrations are also lower in Core MRS-CS-05 compared to concentrations in Core MRS-CS-16. The significant features are that Fe

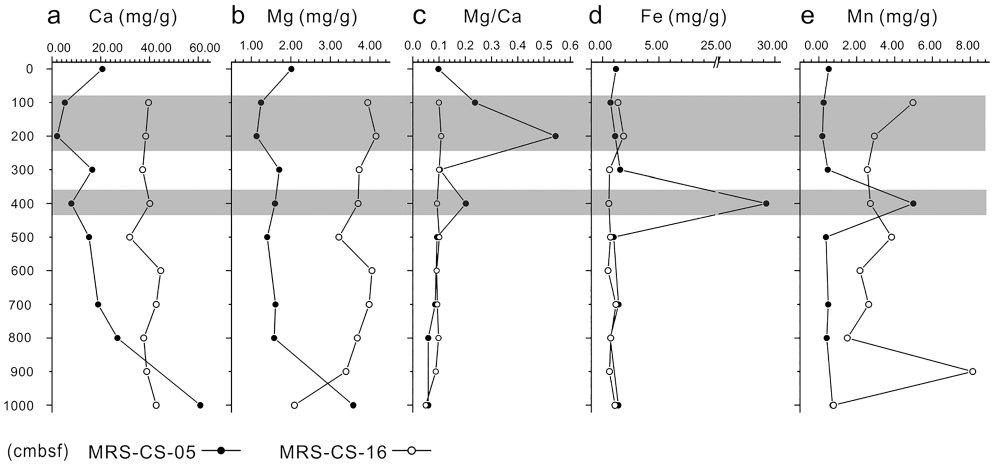

Figure 6. (a) Ca (mg/g), (b) Mg (mg/g), (c) Mg/Ca (mg/mg), (d) Fe (mg/g), and (e) Mn (mg/g) from Cores MRS-CS-05 and MRS-CS-16. Filled and open circles represent the two cores. The upper shaded areas indicate the high Mg/Ca ratios, and the lower shaded areas indicate the high Fe, Mn contents in Core MRS-CS-05. cmbsf = centimeters below seafloor.

and Mn concentrations in Core MRS-CS-05 exhibit extremely high values of 29.24 and 4.99 mg/g, respectively, at the depth of 400 cmbsf, while Mn concentrations in Core MRS-CS-16 show a maximum value of 8.13 mg/g at 800 cmbsf without a notable change in Fe concentrations (Figure 6).

4.4. Strontium Isotopes

The $^{87}Sr/^{86}Sr$ ratios in Core MRS-CS-05 show an extremely high value of 0.709042 at 1,000 cmbsf, followed by a sharp decline to 0.708478 at 800 cmbsf, and then keep comparatively constant values from 800 to 400 cmbsf (Figure 7). The transition from 400 to 300 cmbsf is marked by a steep rise to 0.708916. Above 300 cmbsf, the ratio progressively decreases to 0.708316 at the seafloor. In Core MRS-CS-16, the $^{87}Sr/^{86}Sr$ ratios are stable from 900 cmbsf to the seafloor, varying between 0.708798 and 0.708886.

The $^{87}Sr/^{86}Sr$ ratios of bulk carbonates in Cores MRS-CS-05 and MRS-CS-16 are generally lower than those of mollusk shells (0.70916 and 0.70898 for marine and freshwater species, respectively) on the Western High (Vidal et al., 2010). This is likely due to the presence of detrital carbonates of Paleogene/Neogene age that lower the original biogenic $^{87}Sr/^{86}Sr$ (Cox & Faure, 1974; Major et al., 2006).

5. Discussion

5.1. Geochemical and Mineralogical Characteristics of Bulk Carbonates

5.1.1. Components of Bulk Carbonates in Two Sites

Bulk carbonates in sediments are often composed of a mixture of different components. The authigenic carbonates with their well-developed morphologies were identified through SEM observations in Core MRS-CS-05 (Figure 4). These include the acicular crystals of aragonite (Figure 4a), blade-like crystals of siderite (Fe-rich calcite; Figures 4b, 4c, S3, and S4), and platy crystals of Mg-calcite (Figure S2). The SEM observations, together with energy diffraction spectrum data, correspond well with the elemental concentrations of the bulk carbonates in cores, with aragonite-rich levels characterized by high-Mg at depths of 100, 200, and 400 cmbsf and Fe-rich calcites with apparent high Mg/Ca and high Fe,Mn at depths of 400 cmbsf (Figure 6 and section 5.1.2). As for biogenic carbonates, no foraminifera is identified in Core MRS-CS-05, while the widespread occurrence of foraminifera, with calcite composition, is confirmed in Core MRS-CS-16.

The contribution of biogenic, authigenic, and detrital carbonates to bulk carbonates were investigated with a mixing model in which four end member ratios of Sr/Ca and Mg/Ca were used (Bayon et al., 2007; Çağatay et al., 2017; Fontanier et al., 2018; Figure 8). The results from MRS-CS-16 follow a mixing line between detrital calcite and biogenic calcite. Results from MRS-CS-05 do not follow a mixing line and instead are interpreted to be composed of a mixture of high Mg-calcite and aragonite of authigenic origin.

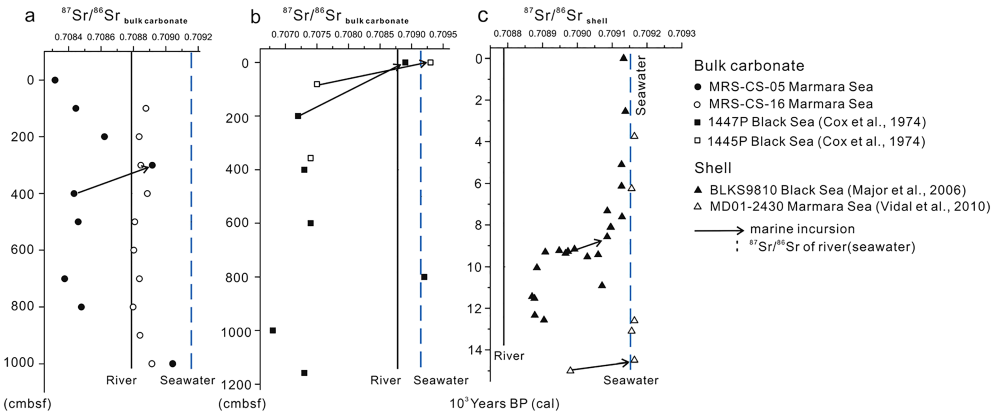

Figure 7. Comparison of $^{87}Sr/^{86}Sr$ of bulk carbonates and shells from the Sea of Marmara and the Black Sea: (a) $^{87}Sr/^{86}Sr_{bulk\ carbonate}$ of Cores MRS-CS-05 and MRS-CS-16 from the Western High and the Çınarcık Basin of Marmara Sea; (b) $^{87}Sr/^{86}Sr_{bulk\ carbonate}$ of Cores 1445P and 1447P from the Black Sea (Cox & Faure, 1974); (c) $^{87}Sr/^{86}Sr_{shell}$ of mixed cores from the Black Sea (Major et al., 2006) and of Core MD01-2430 from the Marmara Sea (Vidal et al., 2010). cmbsf = centimeters below seafloor.

5.1.2. Partial Dissolution of Primary Carbonates

The depletion of carbonate-bound Mg and Ca concentrations were observed at the sedimentary horizons 100, 200, and 400 cmbsf in Core MRS-CS-05 (Figure 6). Powdered X-ray diffractograms (PXRD) of sediments also reveal that the carbonate phase disappeared at 100, 200, and 400 cmbsf (Figure 3a), supporting the dissolution of primary carbonates in the acidic environment. In addition, during our sediment sieving and manual picking, no foraminifera was identified in Core MRS-CS-05, which can also be attributed to the dissolution of primary carbonates. Partial dissolutions of carbonate minerals in the SoM have also been observed in surficial carbonates due to acidity created by pyrite oxidation (Crémière, Pierre, et al., 2012). The fundamental parameter that influences calcium carbonate dissolution is the carbonate saturation state of pore water (Morse et al., 2007), which is mainly controlled by pH and alkalinity of pore water. Experimental studies have revealed that pH is a critical factor influencing the carbonate saturation state in sediments, with low pH leading to the dissolution of carbonates (Waldbusser et al., 2011). In the Western High, the sedimentary environment with low pH is created by anaerobic biodegradation of seeping petroleum, a phenomenon recognized by the occurrence of greigite (Yang et al., 2018). Greigite is formed in anoxic environments with a pH less than 5 (Roberts & Weaver, 2005), where carbonates, and primarily foraminifera, are dissolved.

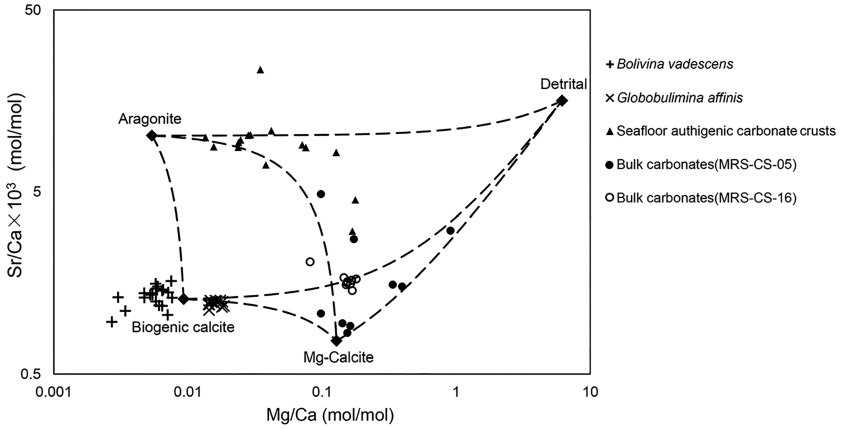

Figure 8. Relationship between Mg/Ca and Sr/Ca (mol ratio) in seafloor authigenic carbonate crusts (Çağatay et al., 2017), benthic foraminifera (Fontanier et al., 2017), and bulk carbonate in sediments from the Marmara Sea (this study). The dashed lines correspond to mixing lines between hypothetical end-members: terrigenous material, aragonite, Mg-calcite, and biogenic calcite. Modified from Bayon et al. (2007).

5.1.3. Formation of Authigenic Carbonates

All the data sets presented in section 5.1.2 collectively support our hypothesis that the primary carbonates are dissolved by the acidic fluids in Core MRS-CS-05, and the authigenic carbonates precipitate later (Figure 8). The newly formed authigenic carbonates include high-Mg calcite, aragonite, and siderite, which are identified by their fine morphology under SEM, as described in section 5.1.1 and illustrated in Figures 4 and S1–S4. These carbonate minerals are formed by the well-known process of the coupled AOM and sulfate reduction, which lead to the authigenic carbonate precipitation at or near the seafloor by increasing the alkalinity (see section 1 and references therein). The same processes have been demonstrated in the SoM by previous studies (Çağatay et al., 2017; Crémière et al., 2013; Crémière, Pierre, et al., 2012; Ruffine et al., 2015), and the possible source of carbon are discussed in the next section.

5.1.4. Implication for Carbon Sources of the DIC Pool

Bulk carbonates from sediments on the Western High exhibit a wide range of $\delta^{13}C$ values from −1.7‰ to +24.3‰ VPDB, indicating a complex mixture of multiple DIC sources in diagenetic fluids. It is noteworthy that the $\delta^{13}C_{bulk\ carbonate}$ as positive as +24.3‰ VPDB at 400 cmbsf (Figure 4) is almost identical to the signature of CO_2 ($\delta^{13}C$ of 28.4–29.1‰ VPDB) in the emitted gas bubbles from the Western High (Ruffine, Donval, et al., 2018), reflecting mineralization of the isotopically enriched CO_2 (Figure 9).

CO_2 derived by anaerobic petroleum degradation can undergo secondary methanogenesis in subsurface reservoirs. The initial carbon dioxide is highly enriched in $\delta^{13}C$ (Jones et al., 2008; Masterson et al., 2001; Pallasser, 2000). Methanogenesis through petroleum biodegradation starts with syntrophic alkane oxidation (equation (1)) and results in the production of CO_2 from syntrophic acetate oxidation (equation (2)). The associated H_2 released is then taken up in the transformation of CO_2 to methane when petroleum degradation is followed by methanogenesis (equation (3); Jones et al., 2008):

$$4C_{16}H_{34} + 64H_20 \rightarrow 32CH_3COO^- + 32H^+ + 68H_2, \quad (1)$$

$$32CH_3COO^- + 32H_2 + 64H_2O \rightarrow 128H_2 + 64CO_2, \quad (2)$$

$$196H_2 + 64CO_2 \rightarrow 49CH_4 + 15CO_2 + 98H_2O \quad (3)$$

CO_2 becomes isotopically enriched with increasing hydrocarbon conversion (Jones et al., 2008). For example, biochemical fractionation of degraded petroleum resulted in a kinetic isotopic shift to 13.05–18.05‰ VPDB in the Peace River petroleum sands, which is supported by the theoretical study (Jones et al., 2008), and similar phenomena identified in the Gippsland and Otway Basins (Pallasser, 2000). As referred to those literature results, the ^{13}C-enriched CO_2 generated in the Western High of the SoM attests an origin of petroleum biodegradation, which is interpreted to reflect the petroleum migration from the Thrace Basin through the NW-SE strike-slip and WSW-ENE oblique faults (Bourry et al., 2009; Gürgey et al., 2005).

The $\delta^{13}C$ values of bulk carbonates from SoM (this study) and the Black Sea (Deuser, 1972; Major et al., 2002), as well as $\delta^{13}C$ values of buried and seafloor authigenic carbonates from SoM (Çağatay et al., 2017; Crémière et al., 2013; Crémière, Ponzevera, & Pierre, 2012) are plotted in Figure 9. Apart from the extremely high $\delta^{13}C_{bulk\ carbonate}$ value of +24.3‰ VPDB at 400 cmbsf in Core MRS-CS-05, $\delta^{13}C_{bulk\ carbonate}$ values from the SoM fall in the same area with the $\delta^{13}C_{bulk\ carbonate}$ values measured in Black Sea cores. The $\delta^{13}C$ values of bulk carbonates from this two area range from −5‰ to +5‰ VPDB. $\delta^{13}C_{foraminifera}$ obtained on the Western High (MD01-2430; Vidal et al., 2010) also shows similar values as $\delta^{13}C_{bulk\ carbonate}$. However, $\delta^{13}C$ values of the seafloor authigenic carbonates are obviously lower than those of bulk carbonates and foraminifera (Figure 9), indicating the contribution of a source with lighter $\delta^{13}C$ DIC, primarily derived from methane. Both thermogenic ($\delta^{13}C_{CH4} > -57$‰) and biogenic ($\delta^{13}C_{CH4} < -57$‰) methane are depleted in ^{13}C compared to other DIC (Claypool & Kvenvolden, 1983). $\delta^{13}C$ values of the buried authigenic carbonates range from lighter than −50‰ VPDB to heavier than +15‰ VPDB (Figure 9), presenting the most complex mixture of multiple DIC sources (Crémière, Ponzevera, & Pierre, 2012).

5.2. Implications for the Paleoceanographic Events

5.2.1. $^{87}Sr/^{86}Sr$ and $\delta^{18}O$ of Bulk Carbonates in Lacustrine Sediments

The Late Glacial to Holocene sedimentary sequence in the SoM is divided into two stratigraphic units: the upper marine unit and the lower lacustrine unit (Çağatay et al., 2002; Çağatay et al., 2004; Eriş et al.,

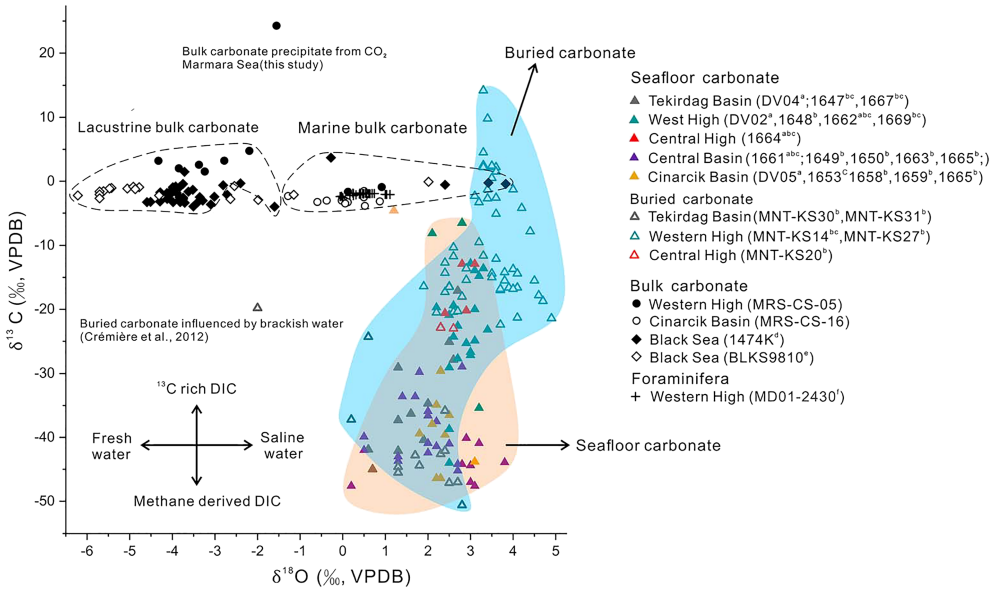

Figure 9. Carbon and oxygen isotopic compositions of seafloor carbonates, buried concretions, shells, and bulk carbonate in sediments. Two dashed line areas are lacustrine bulk carbonate and marine bulk carbonate. The blue shaded area and the orange shaded area are buried carbonate and seafloor carbonate, respectively. (a) Çağatay et al. (2017), (b) Crémière, Pierre, et al. (2012), (c) Crémière et al. (2013), (d) Deuser (1972), (e) Major et al. (2002), and (f) Vidal et al. (2010). VPDB = Vienna Pee Dee Belemnite; DIC = dissolved inorganic carbon.

2012; Vidal et al., 2010). The marine unit is 0–4 m thick on the shelves and structural highs (ridges), while it is more than 10 m thick in the deep basins (Çağatay et al., 2004). This difference is due to the higher sedimentation rates in the deep basins compared to those in the highs and shelves. For example, the marine unit is 3.5 m thick in the 29-m-long Core MD01-2430 from the Western High (Vidal et al., 2010), whereas it is 21.32 m thick in the 32.3-m-long Core MD01-2429 from the Çınarcık Basin (Eriş et al., 2012).

Considering Cores MRS-CS-05 and MD01-2430 are both located on the Western High, they should have experienced similar sedimentation rates, which would also be true for the similarity of sedimentation rates for Cores MRS-CS-16 and MD01-2429 located in the Çınarcık Basin. The difference in the strontium and oxygen isotopic profiles in Cores MRS-CS-05 and MRS-CS-16 (Figures 7 and 10) reveals the difference in the sedimentation rate; the former core includes both an upper marine unit and a lower lacustrine unit, whereas the latter core intercepts only the upper marine unit and fails to penetrate the lower lacustrine unit. In Core MRS-CS-05, the interval from the core bottom to ~400 cmbsf is the lacustrine unit and that from ~400 cmbsf to the seafloor is the marine unit, whereas the whole sedimentary succession in Core MRS-CS-16 belongs to the marine unit.

This conclusion is supported by $^{87}Sr/^{86}Sr$ of the bulk carbonates. In Core MRS-CS-05 on the Western High, $^{87}Sr/^{86}Sr$ of the bulk carbonates in the lacustrine unit from 800 to 400 cmbsf show lower values with less variability (ranging from 0.708376 to 0.708479), than those of the marine sediments above (average: 0.708916), exhibiting the characteristics of sediments deposited in freshwater (Cox & Faure, 1974; Major et al., 2006; Vidal et al., 2010). Freshwater bulk carbonates from the Western High show lower $^{87}Sr/^{86}Sr$ ratios than freshwater shell samples, which is ~0.70898 for freshwater mollusk shells in Core MD01-2430 from the SoM (Vidal et al., 2010) and ~0.7089 for mollusk shells from the Black Sea (Major et al., 2006), reflecting the contribution of the reworked carbonates with low $^{87}Sr/^{86}Sr$ ratio (Cox & Faure, 1974).

$\delta^{18}O_{bulk\ carbonate}$ values decrease gradually from −3.2‰ to −4.3‰ with a 1‰ depletion in the sediments from 800 to 500 cmbsf in Core MRS-CS-05, indicating a stable freshwater environment. This is in good agreement with the results from the benthic ostracod ($\delta^{18}O_{ostr}$) in Core MD01-2430 on the Western High. The $\delta^{18}O_{ostr}$ of approximately −5‰ is nearly constant between 23 and 18 ka BP, indicating a stable hydrologic state during the Last Glacial Maximum, and then a series of meltwater pulses derived from the Eurasian

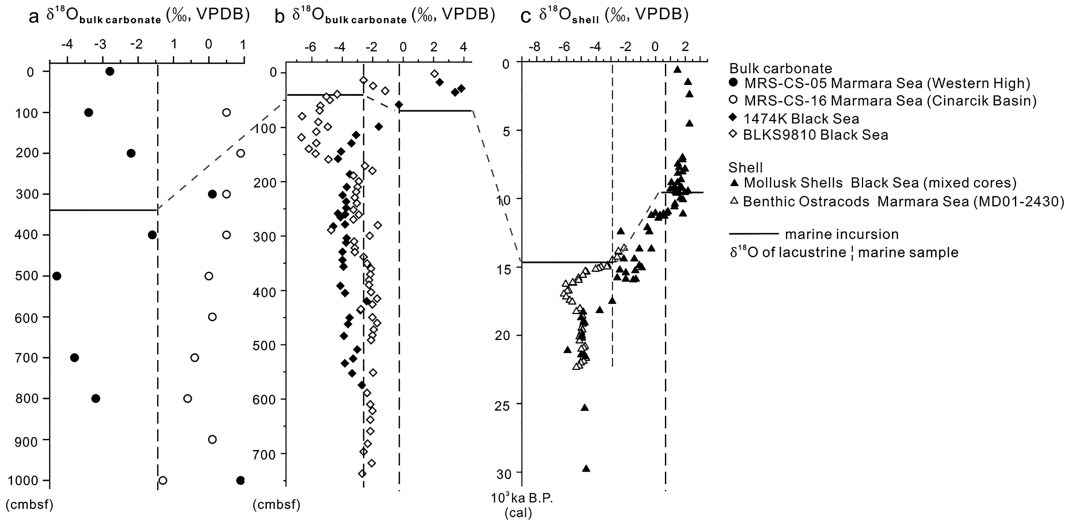

Figure 10. Comparison of oxygen isotopic composition of bulk carbonates and shells from the Marmara Sea and the Black Sea: (a) $\delta^{18}O$ of bulk carbonate of Cores MRS-CS-05 and MRS-CS-16 from the Marmara Sea, (b) $\delta^{18}O$ of bulk carbonate of Core 1474K (Deuser and W., 1972) and Core BLKS9810 (Major et al., 2002) from the Black Sea, (c) $\delta^{18}O_{shell}$ of mollusk shells of mixed cores (three survey areas) from the Black Sea (Major et al., 2006) and $\delta^{18}O_{shell}$ of benthic ostracods (*Candona angulata*) of Core MD01-2430 from the Marmara Sea (Vidal et al., 2010). VPDB = Vienna Pee Dee Belemnite.

ice sheets led to a drop of approximately 1‰ between 18 and 16 ka BP (Vidal et al., 2010). The same uniform trend of $\delta^{18}O_{ostr}$ during the Last Glacial Maximum and a 1‰ depletion during 18.5–15.5 ka BP was also recorded in the Black Sea (Bahr et al., 2006).

5.2.2. $^{87}Sr/^{86}Sr$ and $\delta^{18}O$ of Bulk Carbonates in Marine Sediments

$^{87}Sr/^{86}Sr$ ratios and $\delta^{18}O_{bulk\ carbonate}$ values of bulk carbonate are relatively constant in Core MRS-CS-16. It suggests that the environment of Çınarcık Basin has been stable after the marine incursion. $^{87}Sr/^{86}Sr$ ratios in Core MRS-CS-16 display a steady trend with a mean value of 0.708849, significantly higher than that of 0.708437 in the lacustrine sediments of Core MRS-CS-05. It confirms that the bulk carbonates in Core MRS-CS-16 are derived predominantly from the water of high salinity in a marine environment. Bulk carbonates in sediments from the upper part of Core MRS-CS-05 can also be unambiguously attributed to the marine environment, with a high value of 0.708916.

The trend of the $\delta^{18}O_{bulk\ carbonate}$ variation in Core MRS-CS-16 from the Çınarcık Basin is marked by relatively heavy values (ranging from −0.6‰ to 0.9‰) in the upper part of the core, following with a sharp depletion to −1.3‰ at the bottom (1,000 cmbsf). Such values in the upper sediments are attributed to precipitation from more saline water during the marine stage, given that saline water is isotopically heavy relative to $\delta^{18}O$ depleted brackish water, while the bulk carbonates deposited at 1,000 cmbsf indicate the contribution of ^{18}O-poor brackish water, similar to the low $\delta^{18}O$ value of −1.96‰ for buried concretions observed in the Terkirdağ Basin (Crémière, Ponzevera, & Pierre, 2012; Figure 9).

The $\delta^{18}O$ results of studies on seafloor authigenic carbonate crusts and buried carbonates in the SoM (Çağatay et al., 2017; Crémière et al., 2013; Crémière, Pierre, et al., 2012; Crémière, Ponzevera, & Pierre, 2012) as well as bulk carbonates of the Black Sea sediments (Deuser, 1972; Major et al., 2002), together with the data of current study on bulk carbonates, clearly indicate that the marine bulk carbonates exhibit heavier $\delta^{18}O$ values than lacustrine bulk carbonates, reflecting the contribution of saline water and freshwater, respectively (Figure 9). Moreover, buried carbonates and seafloor carbonates have markedly higher $\delta^{18}O$ values compared to the bulk carbonates, which could be attributed to the inclusion of inorganic calcite formed in the upper $\delta^{18}O$ lighter brackish water layer of the stratified water column.

Table 3
$^{87}Sr/^{86}Sr$ of River and Seawater

Location	$^{87}Sr/^{86}Sr$	Reference
River		
Danube	0.7089	Shimkus and Trimonis (1974) and Palmer and Edmond (1989)
Dniepr	0.7085	Shimkus and Trimonis (1974) and Palmer and Edmond (1989)
Don	0.7085	Shimkus and Trimonis (1974) and Palmer and Edmond (1989)
Sakarya	0.7089	Major et al. (2006)
Seawater		
Global average	0.709155	Henderson et al. (1994) and Broecker and Peng (1982)
Aegean Sea	0.709157	Major et al. (2006)
Marmara Sea	0.709150	Major et al. (2006)
Black Sea	0.7093	Cox and Faure (1974)

5.2.3. Implications for Paleoenvironment Transition

The oxygen isotopic composition of seawater varies mostly through hydrologic mixing process of waters of different salinity (Kaminski et al., 2002; Major et al., 2006). Especially in the SoM, hydrologic processes (precipitation, evaporation, runoff, and marine inflow) rather than temperature changes are the primary causes of $\delta^{18}O$ changes (Vidal et al., 2010).

Over geologic time, $^{87}Sr/^{86}Sr$ ratios in marine sediments change due to different geochemical factors (e.g., soil parent material and water origin) and age; thus, it can be used for chronostratigraphic correlation (Capo et al., 1998; Elderfield, 1986). During the last several thousands of years, seawater $^{87}Sr/^{86}Sr$ ratio has remained stable and homogeneous with a mean value of 0.7092 (Broecker & Peng, 1982; Elderfield, 1986; Henderson et al., 1994). Seawater $^{87}Sr/^{86}Sr$ ratio is distinguishable from river water $^{87}Sr/^{86}Sr$ ratio (Table 3), because the $^{87}Sr/^{86}Sr$ of the river depends on the ages and Rb/Sr ratios of the bedrock and the overburden in the particular drainage basin (Cox & Faure, 1974; Reghizzi et al., 2018). In the SoM, seawaters from the Mediterranean and freshwaters from the Black Sea are the two water sources with significantly different $^{87}Sr/^{86}Sr$ ratios. The seawater $^{87}Sr/^{86}Sr$ ratio for the Aegean Sea is 0.709157 (Major et al., 2006), which can be differentiated from the $^{87}Sr/^{86}Sr$ ratio of 0.7088 for the main river systems draining into the Black Sea (Major et al., 2006; Palmer & Edmond, 1989; Shimkus & Trimonis, 1974). Moreover, the dissolved Sr concentration in seawater is about 30 times higher than that in average river water feeding the Black Sea (Palmer & Edmond, 1989). As a result, water-mass mixing through seawater inflow can induce a detectable shift in the $^{87}Sr/^{86}Sr$ signal in the SoM (Bahr et al., 2008; Major et al., 2006; Vidal et al., 2010).

Both $\delta^{18}O$ values and $^{87}Sr/^{86}Sr$ ratios of bulk carbonates in Core MRS-CS-05 on the Western High vary significantly along the core depth, while they are relatively stable through Core MRS-CS-16 (Figures 7 and 10). The unique combination of $\delta^{18}O$ and $^{87}Sr/^{86}Sr$ allows us to distinguish the marine transition from the earlier lacustrine environment in Core MRS-CS-05. The transition from lacustrine to marine environment has been recognized between 400 and 300 cmbsf of the core with dramatic geochemical changes (Figures 7 and 10). The $^{87}Sr/^{86}Sr$ ratios of bulk carbonates undergo a marked increase from the Late Glacial values, rising abruptly from 0.708434 to 0.708916, caused by the Mediterranean seawater incursion. The $\delta^{18}O_{bulk\ carbonate}$ values increase synchronously by 1.7‰ in 400–300 cmbsf, similar to the increment in $\delta^{18}O_{ostr}$ from the SoM (Vidal et al., 2010) and the Black Sea (Bahr et al., 2006), reflecting the inflow of the Mediterranean seawater.

However, the $\delta^{18}O_{bulk\ carbonate}$ values rise from 500 to 400 cmbsf, which is earlier than the change in the $^{87}Sr/^{86}Sr$ ratio. The absence of variations in the sensitive $^{87}Sr/^{86}Sr$ ratio allowed us to rule out the hypothesis that seawater intrusion occurred during this interval. Then the increase in $\delta^{18}O_{bulk\ carbonate}$ values could have resulted from the progressive salinification caused by excessive evaporation before the Bølling-Allerød warming period (Vidal et al., 2010). On the other hand, gas hydrate destabilization can be an alternative explanation for the higher $\delta^{18}O$ values. Pressure decrease caused by sea/lake water level drop and temperature increase can both lead to the destabilization of gas hydrates in sediments (Davie et al., 2004). Warm and local evaporative conditions in the SoM "lake" during the pre-Bølling-Allerød period (Vidal et al., 2010) may have contributed to the gas hydrate dissociation. The shallow occurrence of gas hydrate in the SoM (Ruffine et al., 2018) makes the gas hydrates even more vulnerable to the temperature and sea level perturbations. Ménot and Bard (2010) found the hopanoid maxima over the last 15 ka and linked it to methanotrophic activity, providing the first geochemical evidence for a large release of methane during the last deglaciation in SoM (Ménot & Bard, 2010). Gas hydrate dissociation can lead to ^{18}O-rich water liberation (Davidson et al., 1983), from which the bulk carbonates with relatively high $\delta^{18}O$ values could precipitate. For a better understanding of the two alternative hypotheses, more sensitive geochemical proxy analyses are planned in the future.

6. Conclusions

The bulk carbonates studied in this research exhibit significant differences in $^{87}Sr/^{86}Sr$ ratios and $\delta^{18}O$ values in marine and lacustrine sedimentary units, primarily associated with the seawater inflow during the deposition process in SoM. These geochemical characteristics can be used to infer major paleoceanographic events across the Late Pleistocene/Holocene lacustrine/marine transition. Both $^{87}Sr/^{86}Sr$ and $\delta^{18}O$ show significant variations in Core MRS-CS-05 from the Western High, caused by the Mediterranean marine incursion during the Late Glacial, while the same ratios are relatively stable in Core MRS-CS-16 from the Çınarcık Basin,

implying stable marine conditions and indicating that the collected core does not bear the lacustrine unit below. This study filled the gap of measurements of $^{87}Sr/^{86}Sr$ on bulk carbonates in SoM, with the results supporting the previous data on carbonate shells. These observations exhibit that hydrologic evolution is discernible from the changes of combined $^{87}Sr/^{86}Sr$ ratios and $\delta^{18}O$ values of the bulk carbonates, similar to that of pure biogenic carbonates such as mollusks and ostracods.

$\delta^{13}C$ and $\delta^{18}O$ values can be additionally used to diagnose the origin of carbonates. Seafloor authigenic carbonates and carbonates buried in shallow sediments deposited under seawater conditions are characterized by heavier $\delta^{18}O$ values (0‰ to 5‰) than the carbonates formed under brackish-water lacustrine conditions (−6.5‰ to −1.5‰). Some marine bulk carbonates of the sediments on the Western High have lighter $\delta^{18}O$ values (−1.5‰ to 2‰), suggesting deposition from lower salinity waters. The $\delta^{13}C$ values of carbonates provide useful information for the recognition of the carbon sources. In general, seafloor carbonates in cold seeps precipitate from the methane-derived DIC and consequently have lighter $\delta^{13}C$ values than those of bulk carbonates with a relatively ^{13}C-rich DIC source. Buried carbonates have the widest range of $\delta^{13}C$ values, probably caused by the mixing of multiple DIC sources. Extremely high $\delta^{13}C$ value (+24.3‰ VPDB) of bulk carbonates in sediments from the Western High was attributed to the mineralization of heavy CO_2, providing independent evidence for the subsurface biodegradation of petroleum.

Primary carbonates were dissolved in Core MRS-CS-05 on the Western High, which was likely caused by an induced acidic environment. The dissolution of both original biogenic carbonates and authigenic carbonates was followed by new authigenic carbonate precipitation. Both high Mg/Ca ratios and SEM identification of aragonite are supportive evidence for the formation of the authigenic carbonates. A less common authigenic carbonate, siderite, was also induced by the AOM and the Fe (and Mn) contained in the hydrocarbon-rich fluids and/or provided by pyrite oxidation. Moreover, based on Sr/Ca and Mg/Ca ratios, the mixing model between the four end members (aragonite, high Mg-calcite, biogenic calcite, and detrital material) suggests that the major components of bulk carbonates in Core MRS-CS-05 are aragonite and high Mg-calcite, while they are biogenic calcite and detrital carbonate material in the bulk carbonates in Core MRS-CS-16.

Acknowledgments
We appreciate the captain and his crew onboard the *RV Pourquoi pas*? and onboard scientists for their support in sampling. All data are included in the supporting information and can be found in the EarthChem Library (https://doi.org/10.1594/IEDA/111338). The financial supports, DD20190234 and HD-JJHT-20 from China Geological Survey and 2017YFC0307603 from Ministry of Science and Technology of the People's Republic of China, to H. L. made this research possible. We would like to express our gratitude to the anonymous reviewers for their constructive comments and suggestions which help improve the manuscript considerably.

References

Aksu, A. E., Hiscott, R. N., Kaminski, M. A., Mudie, P. J., Gillespie, H., Abrajano, T., & Yaşar, D. (2002). Last glacial-Holocene paleoceanography of the Black Sea and Marmara Sea: Stable isotopic, foraminiferal and coccolith evidence. *Marine Geology*, *190*(1-2), 119–149. https://doi.org/10.1016/S0025-3227(02)00345-6

Aloisi, G., Catherine, P., Rouchy, J.-M., Foucher, J.-P., & Woodside, J. (2000). Methane-related authigenic carbonates of Eastern Mediterranean Sea mud volcanoes and their possible relation to gas hydrate destabilisation. *Earth & Planetary Science Letters*, *184*(1), 321–338. https://doi.org/10.1016/S0012-821X(00)00322-8

Armijo, R., Meyer, B., Navarro, S., King, G., & Barka, A. (2002). Asymmetric slip partitioning in the Sea of Marmara pull-apart: A clue to propagation processes of the North Anatolian Fault? *Terra Nova*, *14*(2), 80–86. https://doi.org/10.1046/j.1365-3121.2002.00397.x

Armijo, R., Pondard, N., Meyer, B., Uçarkus, G., de Lépinay, B. M., Malavieille, J., et al. (2005). Submarine fault scarps in the Sea of Marmara pull-apart (North Anatolian Fault): Implications for seismic hazard in Istanbul. *Geochemistry Geophysics Geosystems*, *6*, Q06009. https://doi.org/10.1029/2004GC000896

Bahr, A., Arz, H. W., Lamy, F., & Wefer, G. (2006). Late glacial to Holocene paleoenvironmental evolution of the Black Sea, reconstructed with stable oxygen isotope records obtained on ostracod shells. *Earth & Planetary Science Letters*, *241*(3-4), 863–875. https://doi.org/10.1016/j.epsl.2005.10.036

Bahr, A., Lamy, F., Arz, H. W., Major, C., Kwiecien, O., & Wefer, G. (2008). Abrupt changes of temperature and water chemistry in the late Pleistocene and early Holocene Black Sea. *Geochemistry, Geophysics, Geosystems*, *9*, Q01004. https://doi.org/10.1029/2007gc001683

Bayon, G., Pierre, C., Etoubleau, J., Voisset, M., Cauquil, E., Marsset, T., et al. (2007). Sr/Ca and Mg/Ca ratios in Niger Delta sediments: Implications for authigenic carbonate genesis in cold seep environments. *Marine Geology*, *241*(1-4), 93–109. https://doi.org/10.1016/j.margeo.2007.03.007

Bayrakci, G., Laigle, M., Becel, A., Hirn, A., Taymaz, T., Yolsal-Cevikbilen, S., & team, S. (2013). 3-D sediment-basement tomography of the Northern Marmara trough by a dense OBS network at the nodes of a grid of controlled source profiles along the North Anatolian fault. *Geophysical Journal International*, *194*(3), 1335–1357. https://doi.org/10.1093/gji/ggt211

Birgel, D., Feng, D., Roberts, H., & Peckmann, J. (2011). Changing redox conditions at cold seeps as revealed by authigenic carbonates from Alaminos Canyon, northern Gulf of Mexico. *Chemical Geology*, *285*(1-4), 82–96. https://doi.org/10.1016/j.chemgeo.2011.03.004

Boetius, A., Ravenschlag, K., Schubert, C. J., Rickert, D., Widdel, F., Gieseke, A., et al. (2000). A marine microbial consortium apparently mediating anaerobic oxidation of methane. *Nature*, *407*(6804), 623–626. https://doi.org/10.1038/35036572

Borowski, W., Paull, C., & Ussler, B. (1996). Marine pore-water sulfate profiles indicate in situ methane flux from underlying gas hydrate. *Geology*, *24*(7), 655–658. https://doi.org/10.1130/0091-7613(1996)0242.3.CO;2

Bourry, C., Chazallon, B., Charlou, J. L., Pierre Donval, J., Ruffine, L., Henry, P., et al. (2009). Free gas and gas hydrates from the Sea of Marmara, Turkey: Chemical and structural characterization. *Chemical Geology*, *264*(1-4), 197–206. https://doi.org/10.1016/j.chemgeo.2009.03.007

Broecker, W. S., & Peng, T.-H. (1982). *Tracers in the sea* (p. 690). New York: Lamont-Doherty Geological Observatory.

Çağatay, M. N., Eriş, K., Ryan, W. B. F., Sancar, Ü., Polonia, A., Akçer, S., et al. (2009). Late Pleistocene–Holocene evolution of the northern shelf of the Sea of Marmara. *Marine Geology*, *265*(3-4), 87–100. https://doi.org/10.1016/j.margeo.2009.06.011

Çağatay, M. N., Görür, N., Algan, O., Eastoe, C., Tchapalyga, A., Ongan, D., et al. (2000). Late Glacial–Holocene palaeoceanography of the Sea of Marmara: Timing of connections with the Mediterranean and the Black Seas. *Marine Geology*, *167*(3-4), 191–206. https://doi.org/10.1016/S0025-3227(00)00031-1

Çağatay, M. N., Görür, N., Flecker, R., Sakınç, M., Tünoğlu, C., Ellam, R., et al. (2006). Paratethyan–Mediterranean connectivity in the Sea of Marmara region (NW Turkey) during the Messinian. *Sedimentary Geology*, *188-189*, 171–187. https://doi.org/10.1016/j.sedgeo.2006.03.004

Çağatay, M. N., Keigwin, L. D., Okay, N., Sarı, E., & Algan, O. (2002). Variability of clay-mineral composition on Carolina Slope (NW Atlantic) during marine isotope stages 1–3 and its paleoceanographic significance. *Marine Geology*, *189*(1-2), 163–174. https://doi.org/10.1016/S0025-3227(02)00330-4

Çağatay, M. N., Ozcan, M., & Gungor, E. (2004). Pore-water and sediment geochemistry in the Marmara Sea (Turkey): Early diagenesis and diffusive fluxes. *Geochemistry Exploration Environment Analysis*, *4*(3), 213–225. https://doi.org/10.1144/1467-7873/04-202

Çağatay, M. N., & Ucarkus, G. (2018). Morphotectonics of the Sea of Marmara: Basins and highs on the North Anatolian continental transform plate boundary. In J. Duarte (Ed.), *Transform plate boundaries and fracture zones*. Elsevier; 397–416.

Çağatay, M. N., Wulf, S., Sancar, Ü., Özmaral, A., Vidal, L., Henry, P., et al. (2015). The tephra record from the Sea of Marmara for the last ca. 70 ka and its palaeoceanographic implications. *Marine Geology*, *361*(2), 96–110. https://doi.org/10.1016/j.margeo.2015.01.005

Çağatay, M. N., Yıldız, G., Bayon, G., Ruffine, L., & Henry, P. (2017). Seafloor authigenic carbonate crusts along the submerged part of the North Anatolian Fault in the Sea of Marmara: Mineralogy, geochemistry, textures and genesis. *Deep Sea Research Part II: Topical Studies in Oceanography*, *153*, 92–109. https://doi.org/10.1016/j.dsr2.2017.09.003

Capo, R. C., Stewart, B. W., & Chadwick, O. A. (1998). Strontium isotopes as tracers of ecosystem processes: Theory and methods. *Geofisica Internacional*, *82*(1-3), 197–225. https://doi.org/10.1016/S0016-7061(97)00102-X

Chevalier, N., Bouloubassi, I., Birgel, D., Crémière, A., Taphanel, M. H., & Pierre, C. (2011). Authigenic carbonates at cold seeps in the Marmara Sea (Turkey): A lipid biomarker and stable carbon and oxygen isotope investigation. *Marine Geology*, *288*(1-4), 112–121. https://doi.org/10.1016/j.margeo.2011.08.005

Claypool, G. E., & Kvenvolden, K. A. (1983). Methane and other hydrocarbon gases in marine sediment. *Annu.rev.earth Planet.sci*, *11*(1), 299–327. https://doi.org/10.1146/annurev.ea.11.050183.001503

Cox, J. M., & Faure, G. (1974). Isotope composition of strontium in carbonate phase of two cores from Black Sea. In E. T. Degens, & D. A. Ross (Eds.), *The Black Sea—Geology, chemistry and biology*, (pp. 566–569). Tulsa: American Association of Petroleum Geologists.

Crémière, A., Bayon, G., Ponzevera, E., & Pierre, C. (2013). Paleo-environmental controls on cold seep carbonate authigenesis in the Sea of Marmara. *Earth & Planetary Sciences Letters*, *376*(5), 200–211. https://doi.org/10.1016/j.epsl.2013.06.029

Crémière, A., Pierre, C., Blanc-Valleron, M. M., Zitter, T., Çağatay, M. N., & Henry, P. (2012). Methane-derived authigenic carbonates along the North Anatolian fault system in the Sea of Marmara (Turkey). *Deep Sea Research Part I: Oceanographic Research Papers*, *66*(1), 114–130. https://doi.org/10.1016/j.dsr.2012.03.014

Crémière, B. G., Ponzevera, E., & Pierre, C. (2012). Geochronology and stable isotope geochemistry of cold-seep carbonates from the Sea of Marmara. Paper presented at the EGU.

Davidson, D. W., Leaist, D. G., & Hesse, R. (1983). Oxygen-18 enrichment in the water of a clathrate hydrate. *Geochimica Et Cosmochimica Acta*, *47*(12), 2293–2295. https://doi.org/10.1016/0016-7037(83)90053-4

Davie, M. K., Zatsepina, O. Y., & Buffett, B. A. (2004). Methane solubility in marine hydrate environments. *Marine Geology*, *203*(1-2), 177–184. https://doi.org/10.1016/S0025-3227(03)00331-1

Deuser, W. G. (1972). Late-Pleistocene and Holocene history of the Black Sea as indicated by stable-isotope studies. *Journal of Geophysical Research*, *77*(6), 1071–1077. https://doi.org/10.1029/JC077i006p01071

Dupré, S., Scalabrin, C., Grall, C., Augustin, J. M., Henry, P., Şengör, A. M. C., et al. (2015). Tectonic and sedimentary controls on widespread gas emissions in the Sea of Marmara: Results from systematic, shipborne multibeam echo sounder water column imaging. *Journal of Geophysical Research: Solid Earth*, *120*, 2891–2912. https://doi.org/10.1002/2014JB011617

EIE. (1993). Sediment data and sediment transport amounts for surface waters in Turkish rivers. General Directorate of State Electric Services, EIE, Ankara. Rep 93–59 https://doi.org/10.1139/e89-165, 26, 10, 1953, 1963

Elderfield, H. (1986). Strontium isotope stratigraphy. *Palaeogeography Palaeoclimatology Palaeoecology*, *57*(1), 71–90. https://doi.org/10.1016/0031-0182(86)90007-6

Eriş, K. K., Çağatay, N., Beck, C., Lepinay, B. M. d., & Corina, C. (2012). Late-Pleistocene to Holocene sedimentary fills of the Çınarcık Basin of the Sea of Marmara. *Sedimentary Geology*, *281*, 151–165. https://doi.org/10.1016/j.sedgeo.2012.09.001

Fontanier, C., Dissard, D., Ruffine, L., Mamo, B., Ponzevera, E., Pelleter, E., ... Savignac, F. (2017). Living (stained) deep-sea foraminifera from the Sea of Marmara: A preliminary study. *Deep Sea Research Part II: Topical Studies in Oceanography*, *153*, 61-78. doi:https://doi.org/10.1016/j.dsr2.2017.12.011

Fontanier, C., Dissard, D., Ruffine, L., Mamo, B., Ponzevera, E., Pelleter, E., et al. (2018). Living (stained) deep-sea foraminifera from the Sea of Marmara: A preliminary study. *Deep Sea Research Part II: Topical Studies in Oceanography*, *153*, 61–78. https://doi.org/10.1016/j.dsr2.2017.12.011

Friedman, I., O'Neil, J.R., 1977. Compilation of stable isotope fractionation factors of geochemical interest. *Data of Geochemistry. U.S. Geological Survey Professional Paper 440-KK*, 6th ed.

Görür, N., & Elbek, Ş. (2013). Tectonic events responsible for shaping the Sea of Marmara and its surrounding region. *Geodinamica Acta*, *26*(1-2), 1–11. https://doi.org/10.1080/09853111.2013.859346

Gürgey, K., Philp, R. P., Clayton, C., Emiroğlu, H., & Siyako, M. (2005). Geochemical and isotopic approach to maturity/source/mixing estimations for natural gas and associated condensates in the Thrace Basin, NW Turkey. *Applied Geochemistry*, *20*(11), 2017–2037. https://doi.org/10.1016/j.apgeochem.2005.07.012

Henderson, G. M., Martel, D. J., O'Nions, R. K., & Shackleton, N. J. (1994). Evolution of seawater $^{87}Sr/^{86}Sr$ over the last 400 ka: The absence of glacial/interglacial cycles. *Earth & Planetary Science Letters*, *128*(3-4), 643–651. https://doi.org/10.1016/0012-821X(94)90176-7

Hinrichs, K.-U., Hayes, J., Sylva, S., G Brewer, P., & F DeLong, E. (1999). Methane-consuming Archaebacteria in marine sediments. *Nature*, *398*(6730), 802–805. https://doi.org/10.1038/19751

Hiscott, R. N., & Aksu, A. E. (2002). Late Quaternary history of the Marmara Sea and Black Sea from high-resolution seismic and gravity-core studies. *Marine Geology*, *190*(1-2), 261–282. https://doi.org/10.1016/S0025-3227(02)00350-X

Hiscott, R. N., Aksu, A. E., Yaşar, D., Kaminski, M. A., Mudie, P. J., Kostylev, V. E., et al. (2002). Deltas south of the Bosphorus Strait record persistent Black Sea outflow to the Marmara Sea since ~10 ka. *Marine Geology*, *190*(1-2), 95–118. https://doi.org/10.1016/S0025-3227(02)00344-4

Israelson, C., & Buchardt, B. (1999). Strontium and oxygen isotopic composition of East Greenland rivers and surface waters: Implication for palaeoenvironmental interpretation. *Palaeogeography, Palaeoclimatology, Palaeoecology*, *153*(1-4), 93–104. https://doi.org/10.1016/S0031-0182(99)00068-1

Jones, D. M., Head, I. M., Gray, N. D., Adams, J. J., Rowan, A. K., Aitken, C. M., et al. (2008). Crude-oil biodegradation via methanogenesis in subsurface petroleum reservoirs. *Nature*, *451*(7175), 176–180. https://doi.org/10.1038/nature06484

Kaminski, M. A., Aksu, A., Box, M., Hiscott, R. N., Filipescu, S., & Al-Salameen, M. (2002). Late Glacial to Holocene benthic foraminifera in the Marmara Sea: Implications for Black Sea–Mediterranean Sea connections following the last deglaciation. *Marine Geology*, *190*(1-2), 165–202. https://doi.org/10.1016/S0025-3227(02)00347-X

Kirci-Elmas, E., Algan, O., Özkar-Öngen, Z., Altenbach, A. V., Sagular, S. K., & Struck, U. (2008). Palaeoenvironmental investigation of sapropelic sediments from the Marmara Sea: A biostratigraphic approach to palaeoceanographic history during the Last Glacial-Holocene. *Turkish Journal of Earth Sciences*, *101*(S1), 127–155. https://doi.org/10.1007/s00015-008-1289-6

Major, C., Ryan, W., Lericolais, G., & Hajdas, I. (2002). Constraints on Black Sea outflow to the Sea of Marmara during the last glacial–interglacial transition. *Marine Geology*, *190*(1-2), 19–34. https://doi.org/10.1016/s0025-3227(02)00340-7

Major, C. O., Goldstein, S. L., Ryan, W. B. F., Lericolais, G., Piotrowski, A. M., & Hajdas, I. (2006). The co-evolution of Black Sea level and composition through the last deglaciation and its paleoclimatic significance. *Quaternary Science Reviews*, *25*(17-18), 2031–2047. https://doi.org/10.1016/j.quascirev.2006.01.032

Masterson, W. D., Dzou, L. I. P., Holba, A. G., Fincannon, A. L., & Ellis, L. (2001). Evidence for biodegradation and evaporative fractionation in West Sak, Kuparuk and Prudhoe Bay field areas, North Slope, Alaska. *Organic Geochemistry*, *32*(3), 411–441. https://doi.org/10.1016/S0146-6380(00)00187-X

Ménot, G., & Bard, E. (2010). Geochemical evidence for a large methane release during the last deglaciation from Marmara Sea sediments. *Geochimica Et Cosmochimica Acta*, *74*(5), 1537–1550. https://doi.org/10.1016/j.gca.2009.11.022

Morse, J., Arvidson, R., & Luttge, A. (2007). Calcium carbonate formation and dissolution. *Chemical Reviews*, *107*(2), 342–381. https://doi.org/10.1021/cr050358j

Neymark, L., Premo, W., N. Mel'nikov, N., & Emsbo, P. (2014). Precise determination of δ88Sr in rocks, minerals, and waters by double-spike TIMS: A powerful tool in the study of geological, hydrological and biological processes.

Orphan, V., House, C., Hinrichs, K.-U., McKeegan, K., & DeLong, E. (2001). Orphan VJ, House CH, Hinrichs K-U, McKeegan KD, DeLong EF.. Methane-consuming Archaea revealed by directly coupled isotopic and phylogenetic analysis. *Science*, *293*, 484–487. https://doi.org/10.1126/science.1061338

Özsoy, E., & Ünlüata, Ü. (1997). Oceanography of the Black Sea: A review of some recent results. *Earth-Science Reviews*, *42*(4), 231–272. https://doi.org/10.1016/S0012-8252(97)81859-4

Pallasser, R. J. (2000). Recognising biodegradation in gas/oil accumulations through the $\delta^{13}C$ compositions of gas components. *Organic Geochemistry*, *31*(12), 1363–1373. https://doi.org/10.1016/S0146-6380(00)00101-7

Palmer, M. R., & Edmond, J. M. (1989). The strontium isotope budget of the modern ocean. *Earth & Planetary Science Letters*, *92*(1), 11–26. https://doi.org/10.1016/0012-821X(89)90017-4

Pierre, C., Demange, J., Blanc-Valleron, M. M., & Dupré, S. (2016). Authigenic carbonate mounds from active methane seeps on the southern Aquitaine Shelf (Bay of Biscay, France): Evidence for anaerobic oxidation of biogenic methane and submarine groundwater discharge during formation. *Continental Shelf Research*, *133*, 13–25. https://doi.org/10.1016/j.csr.2016.12.003

Rangin, C., Demirbag, E., Imren, C., Crusson, A., Normand, A., Drezen, E. L., André, L. B., (2001). Marine Atlas of the Sea of Marmara (Turkey). Data collected on board R. V Le Suroît, September 2000. Retrieved from https://archimer.ifremer.fr/doc/00279/39006/

Reghizzi, M., Lugli, S., Manzi, V., Rossi, F. P., & Roveri, M. (2018). Orbitally forced hydrological balance during the Messinian salinity crisis: Insights from strontium isotopes ($^{87}Sr/^{86}Sr$) in the Vena del Gesso Basin (Northern Apennines, Italy). *Paleoceanography and Paleoclimatology*, *33*(7), 716–731. https://doi.org/10.1029/2018pa003395

Reichel, T., & Halbach, P. (2007). An authigenic calcite layer in the sediments of the Sea of Marmara—A geochemical marker horizon with paleoceanographic significance. *Deep Sea Research Part II: Topical Studies in Oceanography*, *54*(11-13), 1201–1215. https://doi.org/10.1016/j.dsr2.2007.04.008

Roberts, A. P., & Weaver, R. (2005). Multiple mechanisms of remagnetization involving sedimentary greigite (Fe_3S_4). *Earth & Planetary Science Letters*, *231*(3-4), 263–277. https://doi.org/10.1016/j.epsl.2004.11.024

Ruffine, L., Çağatay, M. N., & Géli, L. (2018). Fluids and processes at the seismically active fault zone in the Sea of Marmara. *Deep Sea Research Part II: Topical Studies in Oceanography*, *153*(1-3), 1–3. https://doi.org/https://doi.org/10.1016/j.dsr2.2018.09.011

Ruffine, L., Donval, J.-P., Croguennec, C., Burnard, P., Lu, H., Germain, Y., et al. (2018). Multiple gas reservoirs are responsible for the gas emissions along the Marmara fault network. *Deep Sea Research Part II: Topical Studies in Oceanography*, *153*, 48–60. https://doi.org/10.1016/j.dsr2.2017.11.011

Ruffine, L., Germain, Y., Polonia, A., de Prunelé, A., Croguennec, C., Donval, J.-P., et al. (2015). Pore water geochemistry at two seismogenic areas in the Sea of Marmara. *Geochemistry Geophysics Geosystems*, *16*, 2038–2057. https://doi.org/10.1002/2015gc005798

Shimkus, K. M., & Trimonis, E. S. (1974). Modern sedimentation in Black Sea: Sediments. In E. T. Degens, & D. A. Ross (Eds.), *The Black Sea—Geology, chemistry and biology*, *American Association of Petroleum Geologists*, (pp. 249–278).

Teichert, B. M. A., Chevalier, N., Gussone, N., Bayon, G., Ponzevera, E., Ruffine, L., & Strauss, H. (2018). Sulfate-dependent anaerobic oxidation of methane at a highly dynamic bubbling site in the Eastern Sea of Marmara (Çinarcik Basin). *Deep Sea Research Part II: Topical Studies in Oceanography*, *153*, 79–91. https://doi.org/10.1016/j.dsr2.2017.11.014

Tessier, A., Campbell, P. G. C., & Bisson, M. (1979). Sequential extraction procedure for the speciation of particulate trace metals. *Analytical Chemistry*, *51*(7), 844–851. https://doi.org/10.1021/ac50043a017

Tryon, M. D., Henry, P., Çağatay, M. N., Zitter, T. A. C., Géli, L., Gasperini, L., et al. (2010). Pore fluid chemistry of the North Anatolian Fault Zone in the Sea of Marmara: A diversity of sources and processes. *Geochemistry, Geophysics, Geosystems*, *11*, Q0AD03. https://doi.org/10.1029/2010gc003177

Ünlülata, Ü., Oğuz, T., Latif, M. A., & Özsoy, E. (1990). On the physical oceanography of the Turkish Straits. In L. J. E. Pratt (Ed.), *The physical oceanography of sea straits*, (pp. 25–60). Dordrecht: Kluwer Academic Publishing. https://doi.org/10.1007/978-94-009-0677-8_2

Vidal, L., Ménot, G., Joly, C., Bruneton, H., Rostek, F., Çağatay, M. N., et al. (2010). Hydrology in the Sea of Marmara during the last 23 ka: Implications for timing of Black Sea connections and sapropel deposition. *Paleoceanography*, *25*, PA1205. https://doi.org/10.1029/2009PA001735

Waldbusser, G. G., Steenson, R. A., & Green, M. A. (2011). Oyster shell dissolution rates in estuarine waters: Effects of pH and shell legacy. *Journal of Shellfish Research*, *30*(3), 659–669. https://doi.org/10.2983/035.030.0308

Wall, A. J., Capo, R. C., Stewart, B. W., Phan, T. T., & Guthrie, G. D. (2013). High throughput method for Sr extraction from variable matrix waters and $^{87}Sr/^{86}Sr$ isotope analysis by MC-ICP-MS. *Journal of Analytical Atomic Spectrometry*, *28*(8), 1338–1344. https://doi.org/10.1039/C3JA30350K

Whiticar, M. J. (1999). Carbon and hydrogen isotope systematics of bacterial formation and oxidation of methane. *Chemical Geology*, *161*(1–3), 291–314. https://doi.org/10.1016/S0009-2541(99)00092-3

Yang, H., Lu, H., & Ruffine, L. (2018). Geochemical characteristics of iron in sediments from the Sea of Marmara. *Deep Sea Research Part II: Topical Studies in Oceanography*, *153*, 121–130. https://doi.org/10.1016/j.dsr2.2018.01.010

Zitter, T. A. C., Henry, P., Aloisi, G., Delaygue, G., Çagatay, M. N., Mercier de Lepinay, B., et al. (2008). Cold seeps along the main Marmara Fault in the Sea of Marmara (Turkey). *Deep Sea Research Part I: Oceanographic Research Papers*, *55*(4), 552–570. https://doi.org/10.1016/j.dsr.2008.01.002